frontiers | Frontiers in Materials

TYPE Original Research
PUBLISHED 16 October 2024
DOI 10.3389/fmats.2024.1478418

OPEN ACCESS

EDITED BY
Chang Boon Peng,
Nanyang Technological University, Singapore

REVIEWED BY
Roberto Gonzalez Rodriguez,
Texas Christian University, United States
Marimuthu Karunakaran,
Alagappa Government Arts College, India

*CORRESPONDENCE
Nancy Acelas,
nyacelas@udemedellin.edu.co

RECEIVED 09 August 2024
ACCEPTED 03 October 2024
PUBLISHED 16 October 2024

CITATION
Mosqueda-Prado JB, Pinillos-Bernal E, Ospina-Montoya V, Vásquez-Rendón M, Forgionny A and Acelas N (2024) Valorization of nopal wastes to produce quantum dots: optimizing synthesis and exploring in smart textile applications.
Front. Mater. 11:1478418.
doi: 10.3389/fmats.2024.1478418

Valorization of nopal wastes to produce quantum dots: optimizing synthesis and exploring in smart textile applications

Jesús Baltazar Mosqueda-Prado[1], Esteban Pinillos-Bernal[2], Valentina Ospina-Montoya[3], Mauricio Vásquez-Rendón[2], Angélica Forgionny[3] and Nancy Acelas[3]*

[1]Ingeniería en Nanotecnología, Universidad de la Ciénega del Estado de Michoacán de Ocampo, Sahuayo de Morelos, Mexico, [2]Grupo de Investigación en Diseño – TRIADA, Facultad de Diseño, Universidad de Medellín, Medellín, Colombia, [3]Grupo de Investigación Materiales con Impacto (Mat&mpac), Facultad de Ciencias Básicas, Universidad de Medellín, Medellín, Colombia

Quantum carbon dots (QCDs) were efficiently synthesized from post-extraction residues generated during nopal fabric production using a hydrothermal treatment. These QCDs were applied to nopal fabrics, enhancing their UV solar radiation absorption. The synthesized QCDs exhibited fluorescence emissions in the 200–300 nm range. An eco-friendly dispersion was created by incorporating QCDs into TiO_2 for use in smart textiles, which underlines our commitment to maintaining a sustainable process. Bright and fluorescent patterns were successfully applied to commercial and nopal fabrics using a spray printing technique. Additionally, the QCDs demonstrated pH-sensitive color changes, paving the way for practical applications. This work represents an initial step towards a circular economy by utilizing residues from nopal fabric production to synthesize quantum dots, which may be employed in smart textiles applications with UV absorption capabilities.

KEYWORDS

nopal, waste, quantum dots, titanium oxide, fluorescence sensing, smart textiles

1 Introduction

In recent decades, nanomaterials have emerged as a revolutionary family of materials that positively impact science and technology developments due to their unique properties (Ling et al., 2022). Among these materials, quantum dots (QDs) stand out as structures that exhibit exceptional optical and electronic properties due to their quantum confinement (Zhao et al., 2024), which allows for obtaining new materials with tunable photoluminescence and high photostability. Within this category, special attention has been paid to carbon quantum dots (CQDs). Their primary components are organic, which makes them less toxic than other quantum dots. CQDs offer advantages such as high stability, biocompatibility, and ease of synthesis from abundant and sustainable sources, including those from agroindustry (Franco et al., 2020; Chauhan et al., 2022; Dhamodharan et al., 2022). These characteristics make them particularly attractive for applications in bioimaging, sensors, photocatalysis, anti-counterfeiting, energy storage/conversion, and

other advanced technology and scientific research areas (Wang et al., 2024). The quantum confinement effect in these materials enhances their optical properties and influences their electronic behavior. A distinctive feature of most CQDs is their remarkable photoluminescence under UV light, an optical property that is directly related to their size. This quality enhances an efficient excitation even in range close to 530 nm within the electromagnetic spectrum, further expanding the perspectives of potential applications (Agarwal et al., 2023; Ehtesabi and Kalji, 2024; Lysenko et al., 2024). CQDs' versatility and unique properties, outline them as promising materials for innovation and development of advanced applications in several fields of science and technology.

Some reports describe different synthesis methods of CQDs, ranging from simple chemical procedures to more sophisticated and efficient techniques (Quang et al., 2022; Agarwal et al., 2023; Ashraf and Karahan, 2024; Lyu and Han, 2024). Pyrolysis and hydrothermal synthesis have emerged as efficient and simple techniques for producing CQDs from organic matter. These methods have yielded promising results in controlling nanoparticles' resulting size, their structure, and surface characteristics (Jin et al., 2023). These methodologies involve the transformation of carbonaceous precursors, such as agro-industrial wastes, under carefully controlled temperature and pressure conditions, often in the presence of water. The hydrothermal approach utilizes water as a reaction medium, which can act as both a solvent and a catalyst, promoting the formation of CQDs (Jia and Zhang, 2023; Jin et al., 2023; Zamora-Valencia et al., 2023). Modifying CQDs by pH adjustments is a common strategy to control and optimize their optical and absorption properties. Hence, varying pH can influence CQD's structure, spatial arrangement, and surface charge, affecting their absorption properties in the UV region. This is especially relevant in the textile industry, where CQDs can be used to develop fabrics with advanced properties, such as UV protection, antimicrobial effects, and sensing capabilities.

Prolonged and intense exposure to UV radiation carriages significant risks to human health, potentially causing adverse effects (acute or chronic) on the skin, eyes, and immune system, including the risk of developing skin cancer (Hsieh et al., 2008; Román et al., 2019; Felipe et al., 2022). The last is particularly pronounced for outdoor workers such as farmers, mail carriers, and construction personnel facing extended periods of high UV exposure (Román et al., 2019). Consequently, implementing robust sun safety practices, especially protective clothing, is crucial in mitigating the incidence of occupational skin cancer. Various factors, including density, construction, thickness, elasticity, porosity, color, and the incorporation of UV absorbers, determine the efficacy of fabrics in attenuating UV radiation (Román et al., 2019; Felipe et al., 2022). Recent advances in nanotechnology have led to new ways of enhancing the UV-protective properties of textiles. Particularly, applying nanoparticles of SiO_2, TiO_2, ZnO, ZnO_2, CuO, and Ag during fabric finishing processes, has shown promising advances in significantly improving UV protection and other functional attributes (Román et al., 2019). In this context, CQDs have emerged as a cutting-edge frontier in nanotechnology and materials science. These nanomaterials offer unprecedented opportunities for developing smart textiles that effectively block UV radiation and impart additional functionalities such as antimicrobial resistance, self-cleaning properties, and wrinkle resistance (Afroj et al., 2019; Chauhan et al., 2022; Jia and Zhang, 2023). The integration of CQDs into textile manufacturing represents a response to growing consumer demand for advanced materials with multifunctional capabilities.

This research is framed in the integral use of waste generated in nopal (*Opuntia ficus-indica*) crops in the municipality of Sonsón, Antioquia, in Colombia. Nopal is cultivated in this region exclusively to harvest its fruit, prickly pear, which is the primary economic income of more than 500 families. In order to diversify the use of these crops and give them added value, previous works have explored these waste properties to use them in different applications in design (Builes Vélez et al., 2022). Since nopal exhibits a high content of cellulose, lignin, and mucilage, the most recent exploration includes the development of biopolymers to be applied in the textile industry. This work employs the post-extraction residue as a precursor for synthesizing carbon quantum dots (CQDs) through hydrothermal treatment. These CQDs are then applied to nopal fabrics, enhancing their ability to absorb UV solar radiation. This approach converts what was previously considered waste into valuable nanomaterials, promotes local economic development, and enhances environmental sustainability from new green nanotechnology innovation advances. This project addresses challenges in agricultural waste management and pioneers' innovations in advanced materials, showing a comprehensive utilization model that can be adapted to other regions with similar crops. This approach maximizes the value of agricultural resources and promotes sustainable practices in regional agriculture.

2 Methodology

2.1 Reagents

Most of the chemicals used in this study were analytical grade. The following reagents were employed for material preparation: HCl (Merck, 37%), NaOH (PanReac AppliChem, 98%), and Urea (Merck, 99.5%), TiO_2 (Commercial grade), and ethanol (EMSURE®, absolute).

2.2 Biomass pretreatment

To prepare biopolymers, residues from nopal leaves (cladodes) resulting from pruning crops in Sonsón, Antioquia, were selected. Cladodes were heated and cut into 2 × 2 cm squares, passing through a mechanical extractor and separating the liquid and fiber-rich phases. The liquid phase is combined with polymerizing agents to obtain flexible biopolymers with fabric characteristics, Figure 1. The biomass left with a high cellulose content was subjected to a cleaning and pretreatment process before being used as a precursor for the synthesis of CQDs. The residue was repeatedly washed with 1.0 L portions of distilled water to remove surface impurities, and the washed material was dried in an oven (Memmert) at 105 °C for 12 h. Then, the dried residue was subjected to a two-stage grinding process: a) coarse grinding using an industrial blender and b) fine grinding in a coffee mill until a particle size of less than 200 mm was obtained. Subsequently, an acid treatment was performed. For this,

FIGURE 1
Biopolymer fabrication from nopal wastes: **(A)** Residues from leaves (cladodes) resulting from pruning, **(B)** Nopal mucilage extraction from cladodes and fibrous residues produced, **(C)** Biopolymer demolding and visual elastic properties demonstration, and **(D)** Flexible biopolymer with fabric-like characteristics.

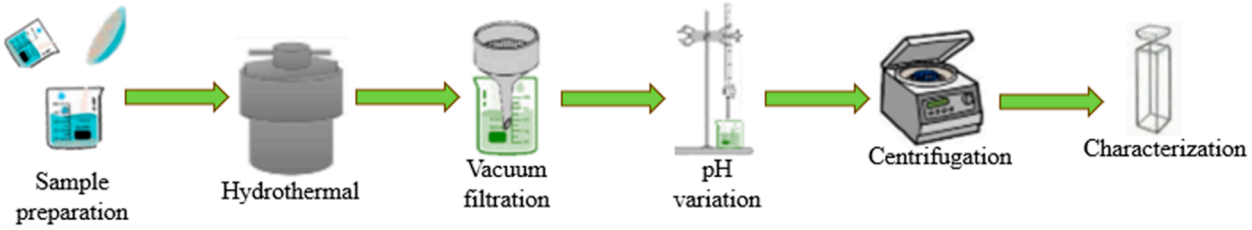

FIGURE 2
Schematic representation of the synthesis process to obtain nopal-derived CQDs.

15.0 g of the ground residue was weighed and mixed with 80 mL of 1.0 M HCl solution. The mixture was placed in an ultrasonic bath for 4 h using an Ultrasonic steam Ultraclean, Elma. After the acid treatment, the sample was washed with deionized water type III at neutral pH. The neutralized material was dried in a conventional oven at 105°C for 2 h. The dry sample was then re-grinded and sieved to a uniform particle size of 0.075 mm using a standard sieve (mesh number 200).

2.3 Synthesis of CQDs

A 1:1 mixture of nopal and urea was prepared by weighing 10 g of nopal and 10 g of urea and dissolved in 120 mL of type II deionized water. The solution was subjected to ultrasound for 30 min to ensure homogeneous dissolution and improve the interaction between the components. The solution was then transferred to a hydrothermal reactor (BAOSHISHAN, BK-series), where it was kept at 180°C during 12 h at an autogenous pressure. Subsequently, the sample was filtered under vacuum to separate the CQDs present in the solution. The filtered solution containing the produced CQDs was adjusted to various pH levels (2, 4, 6, 9, and 12) using 1M HCl and 1M NaOH, where the solution's natural pH is 9. After centrifugation, the presence of CQDs was confirmed using UV light. The procedure used is schematized in Figure 2.

To prepare the solution for spraying on the fabrics, 0.1 g of CQDs was dissolved in 60 mL of ethanol. Then, 1 g of TiO_2 was added to the solution, which was stirred at a controlled temperature until the solvent evaporated completely. The resulting mixture was subjected to pyrolysis for 3 h at 250°C in a horizontal tube furnace with three temperature-controlled zones (model OTP-01, Resistencias y equipos, Colombia), using a heating rate of 10°C/min under an N_2 atmosphere. The sample was stored and labeled CQDs/TiO_2.

2.4 Suspension production of CQD/ TiO_2 and impregnation of textiles

A mass of 100 mg of CQDs/TiO_2 was dispersed in 10 mL of ethanol. This solution was then manually sprayed onto a 2 × 2 cm piece of nopal cloth from a distance of 10 cm. The impregnated textile was then dried in an oven at 45°C for 1 h. This impregnation and drying process was repeated 6 times. Finally, the impregnated textile was examined under UV light to confirm the presence of the CQDs. Figure 3 shows the impregnation sequence of the fabrics. For comparison, a commercial cotton fabric was also impregnated with CQDs/TiO_2. The samples were labeled as nopal fabric (NF) and cotton fabric (CF).

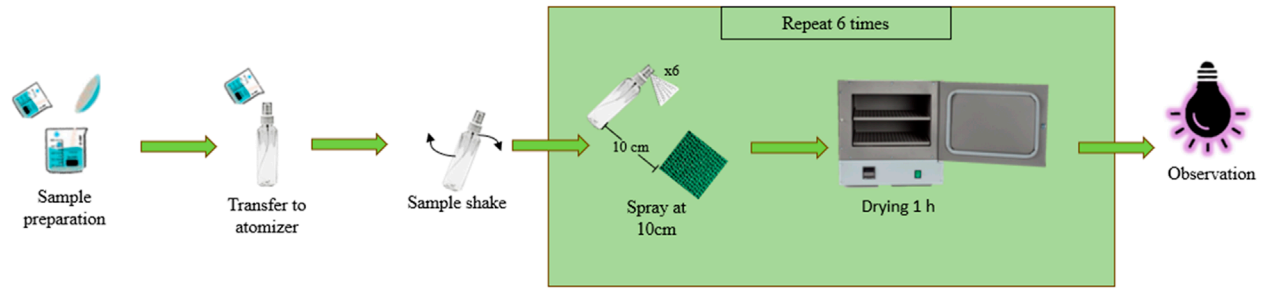

FIGURE 3
$CQDs/TiO_2$ suspension preparation and impregnation process of fabrics for analysis in UV light.

2.5 Materials characterization

2.5.1 Thermal analyses of biomass and biopolymer

Thermogravimetric analysis TGA, was carried out in a TGA Q500 model from TA Instruments. Biomass produced in biopolymer fabrication was dried in a conventional oven at 60 °C for 24 h to remove excessive water content before TGA test. A nitrogen atmosphere was used in a temperature range from 25°C to 700°C, at a heating rate of 10 °C/min.

To evaluate the thermal transitions of nopal biopolymer, a differential scanning calorimetry DSC Q200 from TA Instruments was used. All experiments were set up from −80°C to 220°C at 10 C/min.

2.5.2 Physicochemical and photoluminescence characterization of CQDs and $CQDs/TiO_2$

Several techniques were employed for the physicochemical characterization of CQDs. After synthesis, the filtered CQD solution was visually inspected and exposed to UV light in a radiation chamber. The presence of CQDs was confirmed by the appearance of colored fluorescence in the solution. A PerkinElmer LS-55 spectrofluorometer (Waltham, MA, United States) was utilized to determine the characteristic spectrum of the CQDs. Dispersions of each CQD prepared at a concentration of 100 mg/L in distilled water were introduced into the spectrofluorometer to observe the maximum excitation and emission wavelengths, which are essential for precisely identifying each CQD. Once these specific excitation–emission parameters were established, the fluorescence intensity of each solution was measured. Additionally, to analyze the absorbance properties in the UV-Vis range, a HACH DR-6000 spectrophotometer was used by scanning from 190 to 700 nm dispersing the samples in ethanol. To corroborate that the CQDs particle size is within the nanoscale, that is, below 100 nm, dynamic light scattering (DLS) was employed to determine their hydrodynamic diameter. Tests were conducted in distilled water to assess the stability of these measurements. The analysis was performed using a NanoPlus Zeta/nanoparticle analyzer (Micromeritics, Norcross, GA, United States) at room temperature.

Fourier transform infrared spectroscopy (FT-IR) with attenuated total reflectance (ATR) was performed using a Spectrum Two apparatus (PerkinElmer, Waltham, MA, United States) to identify the functional groups present in the CQDs as a function of solution pH. The samples were analyzed over a 4,000 to 450 cm^{-1} spectral range.

2.5.3 Quantum yield measurement

The quantum yield (Φ) of the synthesized carbon quantum dots (CQDs) was determined using quinine sulphate as a reference, which has a known quantum yield of 0.54 (Arvapalli et al., 2020). To calculate the quantum yield, the integrated photoluminescence intensities and the absorbance values of the CQDs were compared to those of the reference. The quantum yield was then computed using the following equation:

$$\Phi = \Phi_R \frac{I_s A_R \eta_s^2}{I_R A_s \eta_R^2} \quad (1)$$

Where Φ is the quantum yield, I denote the integrated PL intensities, A is the absorbance at the excitation wavelength, η denote the refractive index (1.33 for CQDs and quinine sulphate) (Zhao, 2019; Arvapalli et al., 2020; Goswami et al., 2024), and the subscripts $_S$ refers to CQDs and $_R$ to the reference.

2.6 Morphological and structural characterization of fabrics with $CQDTs/TiO_2$ and particle size distribution of CQDs

The morphology of commercial cotton and nopal fabrics and the dispersion of $CQDTs/TiO_2$ nanoparticles were studied by scanning electron microscopy using a FEI Quanta 600 FEG microscope. Elemental composition of both sample surfaces was analyzed by Energy Dispersive Spectroscopy (EDS). X-ray diffraction (XRD) patterns were obtained using a Shimadzu XRD-6100 diffractometer, utilizing Cu Kα radiation (λ = 1.5406 Å) at an operating voltage of 40 kV. Measurements were conducted over a 2θ angle range of 10°–80° with a step size of 0.026° and a counting period of 50 s per step. The collected data were analyzed to identify crystalline phases and quantify them through Rietveld refinement using High Score Plus software.

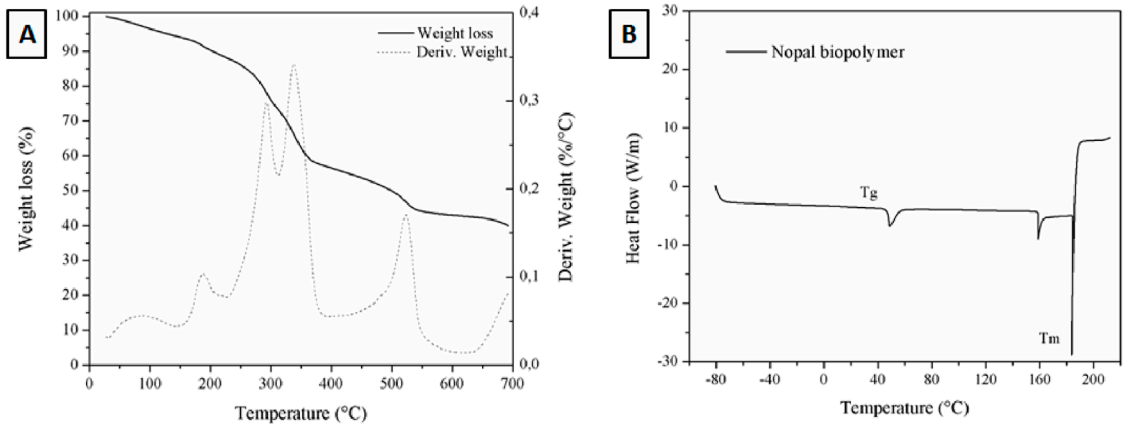

FIGURE 4
(A) Thermogravimetric analysis of biomass produced in nopal biopolymer fabrication. **(B)** Differential scanning calorimetry of nopal biopolymer.

3 Results and discussion

3.1 Thermal analysis of biomass and nopal fabric

Figure 4A exhibits the weight loss by thermal degradation of biomass fibrous residues obtained from mucilage extraction. The first drop is attributed to residual water content left after drying in a conventional oven, followed by step-by-step mass drops due to organic component degradations characteristic of mucilage. After 500°C, it is observed that the fixed carbon left in the sample transforms into residual ashes due to complete degradation of organic matter. These results lead to understanding the processing temperatures that must be used to synthesize the quantum dots from agro-industrial wastes rich in carbonaceous components.

DSC results presented in Figure 4B for nopal biopolymer show the thermoplastic behavior of the material. A first drop in the baseline is observed at 50 °C which is attributed to its glass transition temperature. At 162.5°C, a small peak is noticed, revealing the beginning of the melting temperature of the biopolymer, followed by a drastic drop at 187°C where the sample completely melts. These results support that the material can be processed by temperature to change its shape using different processing techniques from the molten state. In addition, the recommended temperatures to avoid drastic mechanical properties variation are below 50°C. Its flexibility increases if it is heated above this temperature, but it is important not to exceed temperatures above 120°C to prevent the state change from solid to liquid. Additionally, the temperature used to impregnate the quantum dots was below the glass transition temperature, ensuring that the material did not undergo any mechanical or thermal transformation during this process.

3.2 Photoluminescence of CQDs under UV light

Photoluminescence of CQDs is an optical phenomenon in which these nanomaterials emit light when excited by electromagnetic radiation, typically in the UV or visible range. When CQDs are irradiated with high-energy light, electrons in the material absorb this energy and are promoted from the valence band to the conduction band, creating an electron-hole pair (exciton). After excitation, electrons in the conduction band can lose energy through various non-radiative processes until they reach the lowest energy state within the conduction band. Finally, the electrons recombine with the holes in the valence band, emitting the excess energy as photons (light). The wavelength (and, therefore, the color) of the emitted light depends on the size of the QDs due to the quantum confinement effect (Sousa et al., 2021; Ozyurt et al., 2023).

Figures 5A,B show images of the synthesized CQDs under different pH solution conditions captured under visible and UV light exposure, respectively. The results demonstrate a correlation between the solution pH and the CQDs' absorption properties. For instance, the sample at pH 4 exhibited optimal absorption in the UV and near-UV range, visually manifesting as a green-cyan coloration. In contrast, the sample at pH 12 displayed a more intense blue-cyan coloration. This indicates that the CQDs at this higher pH could absorb at lower wavelengths. The distinct visual appearances under the different pH conditions directly reflect the variation in the CQDs absorption characteristics across the electromagnetic spectrum. This pH-dependent tunability of the optical properties is a key feature of these CQDs materials and are consistent with the characteristic photoluminescent properties of CQDs described in the literature (Rivera-Álvarez et al., 2021). Moreover, the relationship between CQD size and emission wavelength suggests that the green-cyan and blue-cyan hues observed are likely attributed to smaller CQDs, approximately in the 2–3 nm range (Pombo Barros, 2011).

To confirm this observation, photoluminescence (PL) spectra (Figure 5C) of the CQDs at different pH levels were obtained, allowing for the identification of their maximum excitation and emission wavelengths. It is well known that the PL spectra and QY are influenced by factors like size, surface functional groups, quantum confinement effects, precursors and their concentrations, synthesis temperature and time, and doping elements (Chang et al., 2023; Sun et al., 2024).

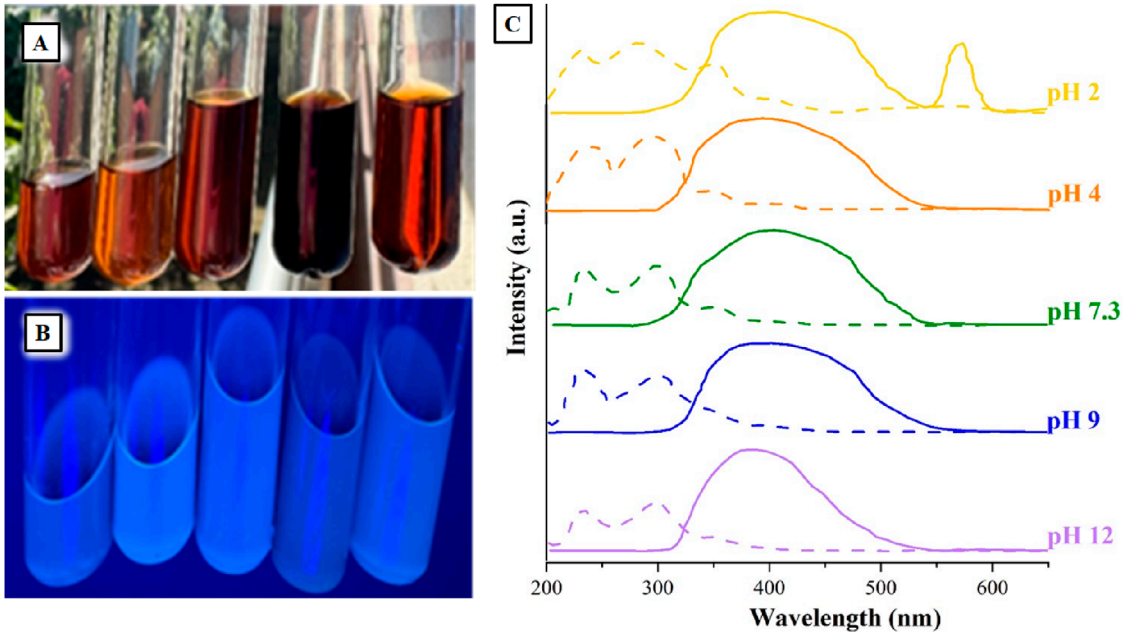

FIGURE 5
Synthetized CQDs dissolved in ethanol at different pH (2, 4, 6, 9, and 12, from left to right), and exposed to two different wavelengths of radiation: **(A)** under visible and **(B)** UV light. **(C)** PL excitation (---), and emission (—) spectra of CQDs at different pH.

CQDs are typically categorized based on their emission color, corresponding to the peak emission wavelength observed in the photoluminescence (PL) spectrum (Goswami et al., 2024). Fluorescence, the underlying optical phenomenon, occurs when fluorophores absorb light at a specific wavelength and re-emit it at a longer wavelength (Mirlou-Miavagh et al., 2024). This process occurs when the electrons in the fluorophore are excited to higher energy levels by absorbing photons (Zhu et al., 2013). In this study, the recorded peak excitation and emission wavelengths were approximately 293–405 nm for CQDs at pH 2, 300–392 nm for CQD at pH 4, 302–404 nm for CQD at pH 6, 302–384 nm for CQD at pH 9 and 301–375 nm for CQD at pH 12. Based on these emission wavelengths, the CQDs would emit light in the violet range of the visible spectrum. Specifically, emission around 400 nm is at the edge between violet and blue, but it is generally classified as violet light (Sun et al., 2024). This observation indicates that the synthesized CQDs exhibit optical properties typical of quantum dots with small particle sizes, where emission shifts toward shorter wavelengths (violet/blue) due to quantum confinement effects. Their ability to emit in the violet range underscores their potential for optoelectronics, bioimaging, and sensing applications, where precise wavelength control is essential (Goswami et al., 2024). These results align with findings from other studies (Goswami et al., 2024), which demonstrate that incorporating heteroatoms, such as nitrogen in N-doped CQDs, induces a blue shift in fluorescence wavelength. Therefore, tuning the fluorescence wavelength, or even the emitted color, is possible by altering the chemical composition or introducing dopants during the CQD synthesis process (Mirlou-Miavagh et al., 2024).

Based on these observations, pH did not significantly affect the fluorescence properties of the CQDs, but it did influence their physical characteristics. Specifically, pH variations impacted the surface charge equilibrium of the CQDs, altering electrostatic interactions between particles, which in turn affected their agglomeration and dispersion in suspension. This was evident in the behavior of the precipitated phases after centrifugation: samples at lower pH (below pH 9) had a higher content of precipitated material. In contrast, the sample at neutral pH exhibited minimal precipitation, and the sample at pH 12 showed almost none. Thus, manipulating pH influenced the colloidal stability and distribution of CQDs in solution and played a crucial role in their agglomeration tendencies.

The quantum yield of the CQDs produced in this study, without pH modification, was calculated using Equation 1 and found to be approximately 58%. This high quantum yield is consistent with values reported for carbon quantum dots synthesized via hydrothermal methods, where uniform particle sizes are typically achieved (Mirlou-Miavagh et al., 2024; Yang et al., 2024). For example, CQDs produced from straw powder under a nitrogen atmosphere at 300°C have been reported to reach yields as high as 64% (Arvapalli et al., 2020). Compared to other biomass-derived CQDs, the quantum yield of the CQDs in this work is significantly higher (Akash et al., 2024). For instance, CQDs derived from strawberry juice through hydrothermal treatment at 120°C had a quantum yield of 6.3%, while sugarcane juice treated under similar conditions yielded 5.76%. Additionally, CQDs from grass treated hydrothermally at 150°C–200°C exhibited quantum yields between 2.5% and 6.2% (Akash et al., 2024). This also demonstrates that quantum dots can be successfully produced from nopal residues left during the biopolymer design using the hydrothermal method.

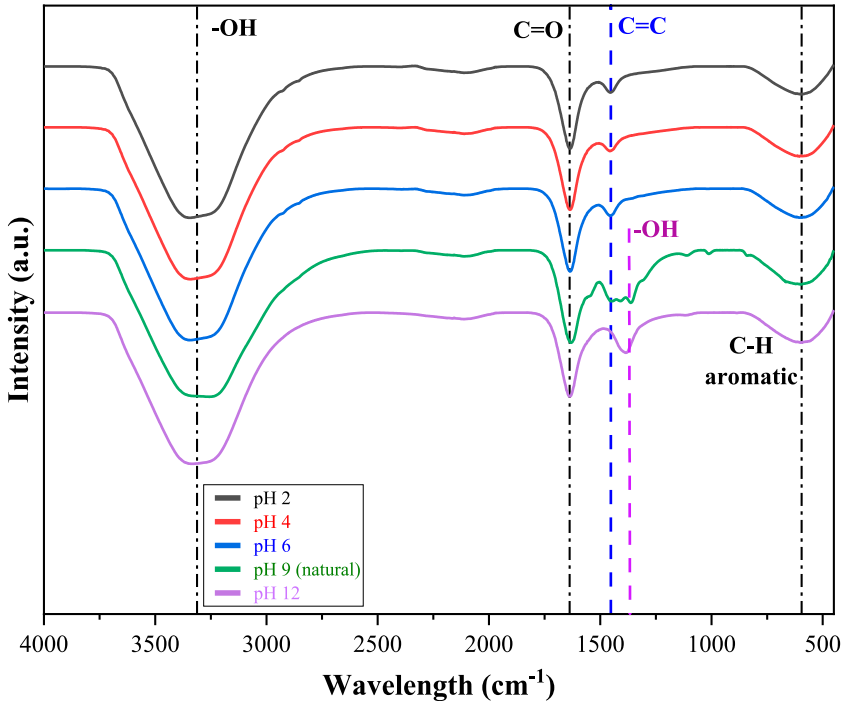

FIGURE 6
FTIR spectra results for CQDs dissolved in ethanol solution with different pH.

3.3 Structural characterization of CQDs and absorption in UV-Vis

FT-IR spectroscopy was used to identify the functional groups present in the CQDs synthesized under different pH conditions (from 2 to 12), (see Figure 6). The spectra reveal structural features and changes induced by pH variation and a general similarity in the spectral profiles between the samples. Nevertheless, some differences are identified for samples at pH 9 and 12, which exhibit additional bands. A broad band centered around 3,321 cm^{-1} is attributed to the stretching vibrations of -OH and N–H groups. Additional bands observed include 1,656 cm^{-1} for C=O, 1,431 cm^{-1} for C=C, 1,355 cm^{-1} for -OH, and 627 cm^{-1} for C-H of aromatic. These bands correspond to various stretching vibrations of functional groups in the CQDs (Sharma and Chowdhury, 2024; Yang et al., 2024).

In particular, the prominent band around 1,431 cm^{-1} observable in all samples, is related to stretching vibrations of sp^2-hybridized C=C bonds, characteristic of aromatic and alkene structures. This finding confirms the presence of graphitic domains in the synthesized CQDs. These bands are more clearly defined in samples at lower pH than natural pH, suggesting an increase of aromatic structures under more acidic conditions. Bands attributable to bending vibrations of C-H bonds in aromatic rings were also observed at 627 cm^{-1}, indicating the presence of aromatic groups. Additionally, the appearance of a band around 1,355 cm^{-1} is characteristic of -O-H bonds. This band suggests the incorporation of electro donating oxygenated group into the structure of the CQDs. The presence of -O-H groups could alter the π-electronic system of the material, which could explain the observed changes in the optical properties of the CQDs as a function of pH (Maiti et al., 2020).

Moreover, spectroscopic and optical results of the CQDs synthesized at pH 12 reveal interesting and complex features. The extended absorption toward the visible spectrum manifested as a more intense blue-cyan coloration, suggests a significant modification in the electronic structure of the CQDs under highly alkaline conditions. The increased absorption intensity in the visible region could be attributed to modification of the π-conjugated structure of the CQDs, since at pH 12, a modification in the extension or configuration of these π-conjugated systems is possible, which could result in a bathochromic (red) shift of the absorption spectrum. The C=C bonds, identified in all samples by FTIR spectroscopy play a key role in the optical properties of CQDs. These bonds enable electronic π-π ∗ transitions that facilitate light absorption in the UV and near-UV region, explaining the efficiency of CQDs as absorbers at these critical wavelengths. This feature is consistent across all samples, regardless of pH, suggesting that these bonds are part of the core structure of CQDs.

In addition, the absorbance spectra for all solutions containing CQDs are shown in Figure 7. The samples have 200–330 nm absorption peaks and extend into the visible region. This wide absorption range allows excitation with broad spectrum light sources, from sources with a high UV index (e.g., sunlight) and low UV index sources (e.g., LED lamps) to visible light. The origin of the peaks from 200–330 nm arose from the electron transitions from π to $\pi*$ from C=C, C=N, and C=O, respectively, as previously reported (Felipe et al., 2022). Besides, it can be observed that the samples at higher pH showed spectra more extended

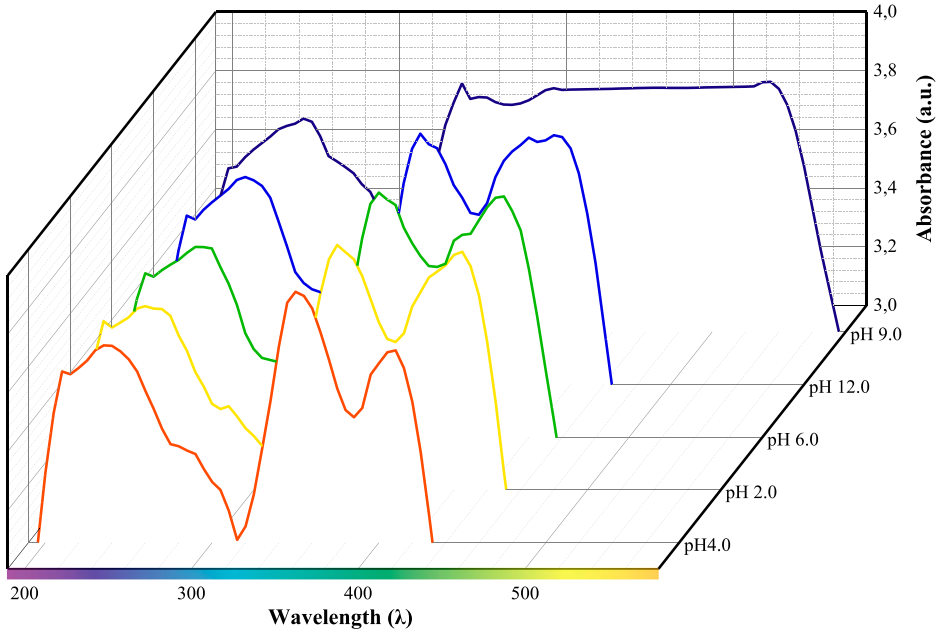

FIGURE 7
UV-Vis Spectrum comparing CQDs absorption at different pH values from 190 to 580 nm. Results are organized from highest to lowest absorption range in the spectrum.

towards the visible region (>400 nm) of the electromagnetic spectrum than those at pH < 9.

This detailed spectroscopic analysis provides valuable information on the chemical composition and structure of the CQDs under different pH conditions. The results indicate that pH variation does not only affects the optical properties of CQDs, as previously observed but also significantly influences their chemical composition. These findings underline the importance of precise control of the chemical environment during the synthesis of CQDs and its effect on the incorporation of specific functional groups into the final structure of the material.

3.4 Characterization of CQDs/TiO_2

3.4.1 FTIR analysis

The FT-IR spectra for the synthesized samples are presented in Figure 8: (A) CQDs in ethanol, (B) CQDs/TiO_2 after pyrolysis treatment, and (C) TiO_2. As previously described in the FTIR spectrum of CQDs was observed a broad band around 3,321 cm^{-1} attributed to -OH and N–H groups. Besides, the bands at 2,888 cm^{-1} (C–H), 1,656 cm^{-1} (C=O), 1,431 cm^{-1} (C=C/N-H), 1,395 cm^{-1} (C–N), 1,323 cm^{-1} (O-NO), 1,044 cm^{-1} (C-O-C), 872 cm^{-1} (C-N), and 627 cm^{-1} (C-H aromatic) are associated with the functional groups present in the CQDs (Sharma and Chowdhury, 2024; Yang et al., 2024). Suspension in ethanol does not induce changes in the spectroscopic characteristics of the CQDs, suggesting that the alcoholic environment does not modify the structure of the CQDs. However, the CQDs/TiO_2 spectra show a decrease in the intensity of the bands associated with the CQDs structure and the appearance of an intense band at 679 cm^{-1} associated with the Ti-O-Ti bonds of TiO_2. The decrease in the intensity of the CQDs bands is related to the interaction generated between the CQDs and TiO_2. In this sense, the pyrolysis treatment is responsible for inducing new interactions and altering the chemistry environment of the CQDs when in contact with TiO_2.

3.4.2 UV-vis analysis

The previous three samples (CQDs, CQDs/TiO_2, and TiO_2) were analyzed by UV-Vis spectroscopy (see Figure 9).

CQDs show high and consistent absorption across the entire UV-Vis spectrum, especially in the lower visible and UV regions. The TiO_2 sample shows the typical absorption curve of the anatase TiO_2 with high intensity at the UV region from 300 to 390 nm (Algadi et al., 2021). However, the TiO_2 sample exhibited a small absorption in the visible light region (>400 nm). The presence of structural defects (like vacancies or interstitials) or impurities can introduce additional energy levels within the band gap, allowing for absorption at longer wavelengths. This phenomenon is associated with the bandgap narrowing observed in TiO_2. This minor absorption band could be attributed to low-energy photons exciting trapped electrons in localized states, which are caused by oxygen vacancies. These vacancies are associated with Ti^{4+} ions located just below the conduction band minimum, as previously reported by Tian et al. (2015) (Tian et al., 2015). Upon the incorporation of CQDs, the fundamental absorption edge of anatase TiO_2 is evident at 385 nm, alongside additional absorption bands for wavelengths greater than 400 nm attributable to CQDs. These findings indicate that the introduction of CQDs onto titanium oxide enhances light absorption characteristics. To corroborate these findings, XRD was performed to further validate the material's crystalline structure and phase composition (see Figure 10). Moreover, CQDs behavior

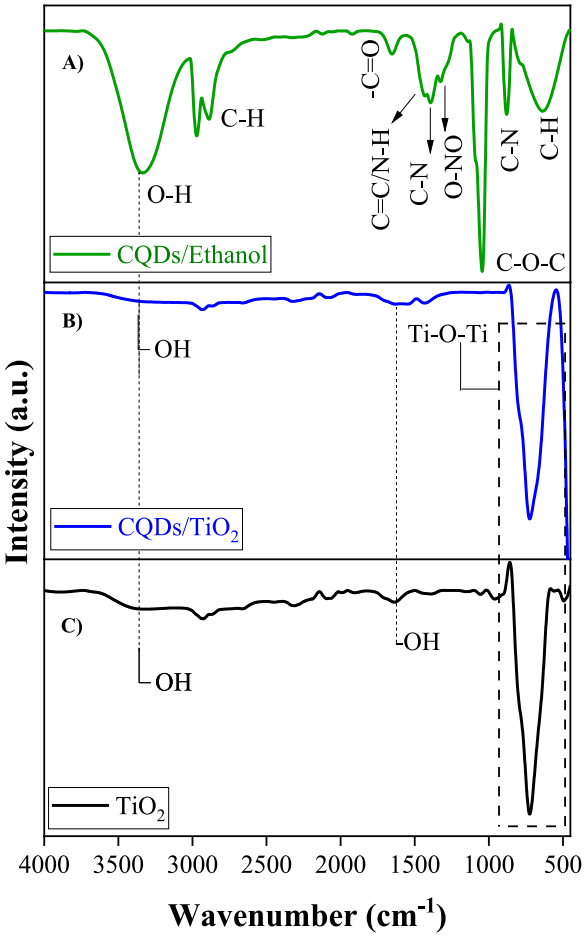

FIGURE 8
Comparative FTIR spectra analysis of samples and a control blank. **(A)** CQDs synthesized and suspended in ethanol, **(B)** CQDs/TiO_2 pyrolyzed, and **(C)** Reference spectrum of TiO_2.

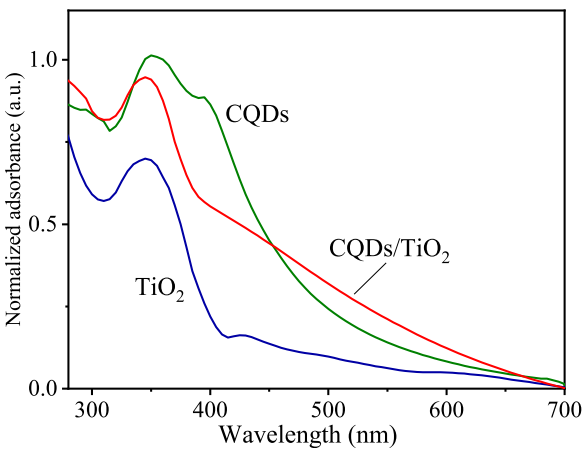

FIGURE 9
UV-Vis absorption spectra for: CQDs, CQDs/TiO_2 and TiO_2 in ethanol.

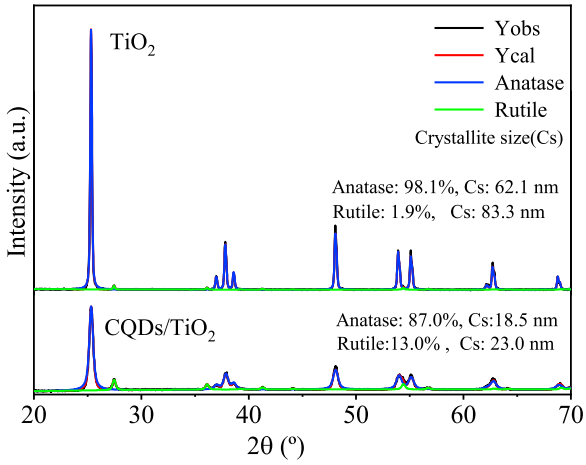

FIGURE 10
XRD of CQDs/TiO_2 and TiO_2.

indicates a high efficiency of light absorption in the UV region, characteristic of their electronic structure and intrinsic optical properties.

Therefore, the CQDs/TiO_2 sample showed a pronounced decrease in absorption observed within the visible region of the UV-Vis spectrum. This change suggests that pyrolysis induces significant transformations in the electronic structure of the CQDs and TiO_2, resulting in a higher excitation in the UV region. The increase in absorption in the UV range could indicate a modification in the electronic transitions and the formation of new absorption centers generated during pyrolysis. Thus, the reduction in absorption in the visible region and the increase in absorption in the UV-C region after pyrolysis suggest a significant transformation in the electronic and optical properties of the CQDs/TiO_2.

3.4.3 XRD analysis

The XRD patterns of the TiO_2 and CQDs/TiO_2 samples are displayed in Figure 10. Seven distinct peaks are observed at 2θ values of 25.305°, 37.871°, 48.023°, 53.976°, 55.049°, 62.728°, and 68.866°. These peaks correspond to the (011), (004), (020), (015), (121), (204), and (116) lattice planes, which belong to the tetragonal anatase phase of TiO_2, as referenced in the ICSD collection code 154604. Also, the peaks at 2θ values of 27.446°, 36.090°, 54.340°, and 69.031° are associated with (110), (011), (121), and (031) lattice plans of tetragonal rutile phase as referenced in the ICSD collection code 169622. However, no distinct peak for CQDs is observed in the CQDs/TiO_2 pattern suggesting a high dispersion of CQDS onto TiO_2, as previously reported (Mahmood et al., 2021; Jin et al., 2023). The incorporation of CQDs into TiO_2 through impregnation and pyrolysis significantly alters the material's structural and phase properties. XRD analysis reveals a notable phase shift, with anatase content decreasing from 98.1% to 87% and rutile increasing from 1.9% to 13%. This transformation suggests that CQDs could act as effective nucleation sites, lowering the energy barrier for the anatase-to-rutile transition during thermal processing. Furthermore, the presence of CQDs constrains crystal growth, resulting in reduced crystallite sizes for both phases. These smaller crystallites enhance

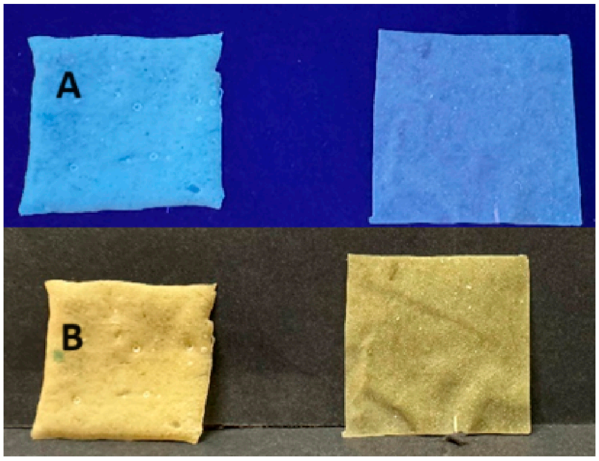

FIGURE 11
Nopal-based fabrics impregnated with a CQDs/TiO_2 solution. **(A)** Under UV light. **(B)** Under visible light.

the material's surface area. The increased formation of the rutile phase reduces structural defects within the solid. Rutile's superior thermal stability compared to anatase promotes a more ordered crystal lattice, typically resulting in fewer defects. Its denser atomic packing minimizes vacancies and interstitials, while the atomic rearrangement during phase transformation further reduces defect density.

3.5 Textile impregnation

3.5.1 Photoluminescence under UV light

Smart textiles are fabrics that modify their properties in response to specific stimuli. A notable category within this field includes fluorescent fabrics that change color upon exposure to light. As shown in Figure 11, the nopal fabric was successfully impregned with CQDs/TiO_2, indicating that this suspension demonstrates photochemical stability. Consequently, these CQDs hold significant potential as effective fluorescent pigments for light-responsive smart textiles.

3.5.2 Structural characterization of CQDs in textiles

After the impregnation process, the fabrics were analyzed by FTIR to evaluate the changes that the CQDs induce in the NF and the CF. No significant changes in the material's structure were observed for the nopal fabric (NF) (see Figure 12). That is, as both the NF and the CQDs are materials of lignocellulosic nature, the presence of typical bands associated with the presence of -O-H, -C-H, C=O and -C-O bonds is observed (as previously discussed in the FTIR spectra of the CQDs). However, variations in the intensity of the peaks in the FT-IR spectra of NF were noted compared to the samples containing the CQDs and CQDs/TiO_2. Impregnated fabrics showed a higher intensity of the bands associated with the functional groups below 3,000 cm^{-1}. These results suggest that the CQDs were incorporated into the fabric, and new interactions were effectively generated between NF and CQDs. This result is corroborated by the image of the impregnated fabrics under UV irradiation and visible light shown in Figure 11, where it is observed that the NF irradiated with UV light exhibits photoluminescence.

For the CF, the FT-IR results showed a similar trend to that observed with NF (see Figure 13). Also, variations in the intensity of the bands were observed in the FTIR spectrum of impregnated fabrics. In this case, the sample impregnated with CQDs showed an improvement in the intensity of the peaks compared to the control sample (CF) and the sample impregnated with CQDs/TiO_2 (CF-CQDs/TiO_2). Unlike the NF, the interaction between the cotton and the CQDs/TiO_2 resulted in a reduction in the intensity of the peaks compared to the control sample. This suggests that the interaction of the CQDs/TiO_2 with the cotton fabric is less effective than NF.

In general, the changes observed in the intensity of the peaks indicate that the impregnation methods successfully modified the surface of the fabrics through CQDs or CQDs incorporation. The enhancement in band intensities for the CQDs-impregnated fabrics suggests an effective interaction between the materials. In contrast, the lower intensity observed with CQDs/TiO_2 might reflect differences in the interaction dynamic between the CQDs/TiO_2 and the textile materials' components.

3.5.3 Morphology of commercial and nopal fabrics, and CQDs impregnation

Figure 14 shows the morphology of commercial fabrics, its impregnation of neat quantum dots, and quantum dots with TiO_2, and the elementary composition of the samples mapped with EDS analysis. In Figure 14A, at a magnification of ×30, it is noticed that cotton threads are woven in a plain weave and that each thread consists of multiple fibers, as it is observed in greater detail at ×250 magnification. Each fiber has a diameter close to 5 μm, and they have a smooth surface, as it is noticed in detail at ×2,500. In Figure 14B, the impregnation of the nanoparticles cannot be identified at ×30 since all the fabrics look the same. However, as the magnification increases, noticeable differences are observed when are added 0.3% of quantum dots. The CQDs particles are distributed along cotton fibers surface; however, they are poorly dispersed and a sectorized agglomeration is noticed along fibers. The dynamic light scattering (DLS) analysis, performed to concentrations between 100 and 500 ppm, revealed the hydrodynamic diameter mean of CQDs is within the nanoscale, close to 77 nm, Supplementary Figure S1. In SEM images there are noticed as aggregates which tend to be significantly greater than the individual particle size, as reported previously by Rosales and coworkers (Rosales et al., 2024). These nanoparticle clusters disappear when including TiO_2, Figure 14C, which acts as a dispersing agent that promotes the homogeneous distribution of the nanoparticles along the surface.

EDS spectra show that the fabric composition is carbon-based, as well as the composition of the CQD at counts that are reported in other works (Mansur and Mansur, 2015; Rasal et al., 2021; Ezati and Rhim, 2022; K. Algethami et al., 2022), and that the presence of titanium is appreciated at a marked peak at 4 keV.

In Figure 15 are presented the SEM and EDS results for nopal fabrics. There are noticed marked differences between the morphology of both, commercial and biopolymer fabrics. The nopal fabric structure is formed by microglobules of different sizes adhered to each other. This pattern has been reported for other authors in biopolymers fabrication from different natural sources (Li et al.,

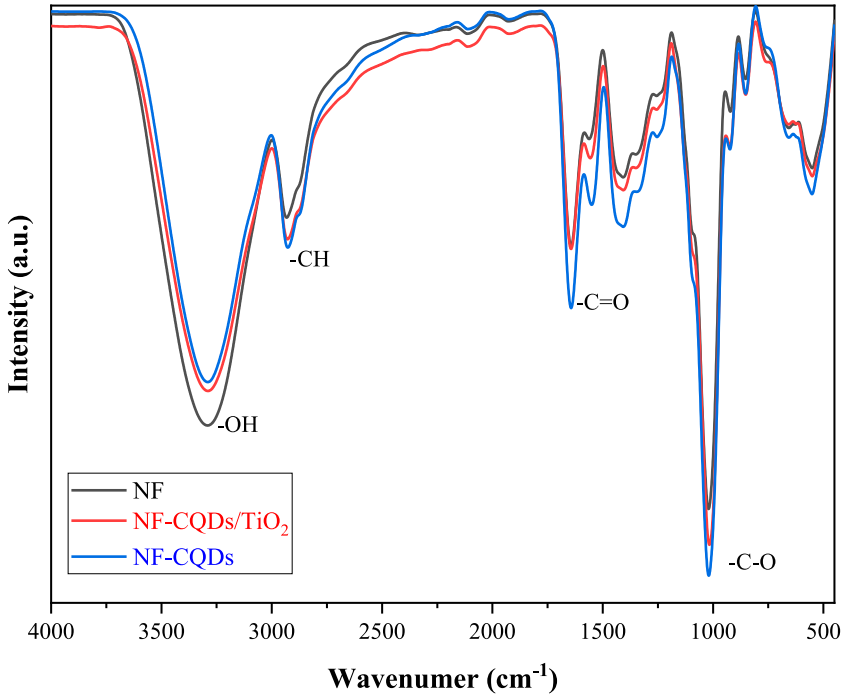

FIGURE 12
Comparative FTIR spectra of NF, and NF impregnated with CQDs and CQDs/TiO_2.

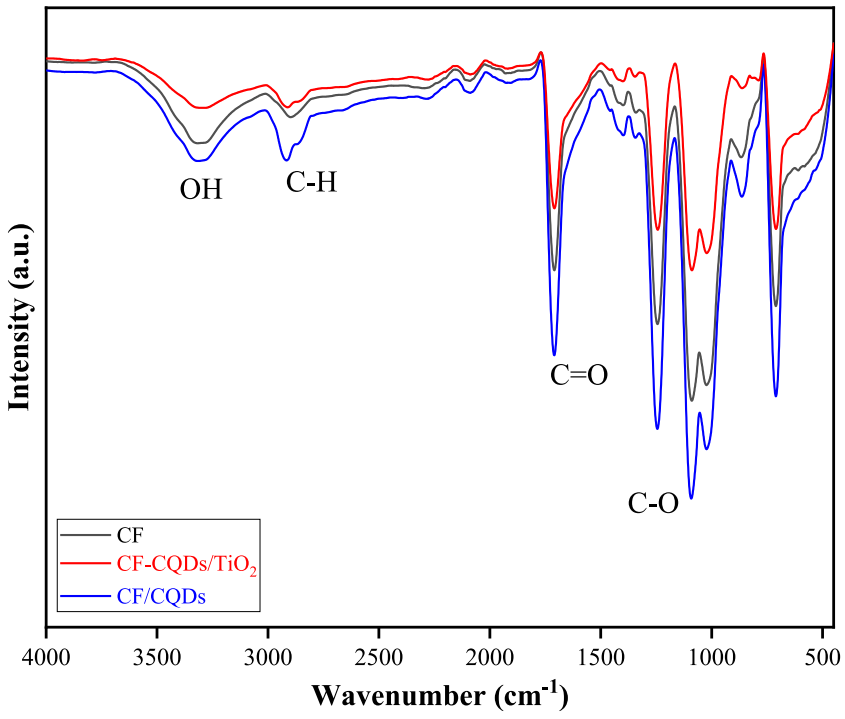

FIGURE 13
Comparative FTIR spectra of CF, and CF impregnated with CQDs and CQDs/TiO_2.

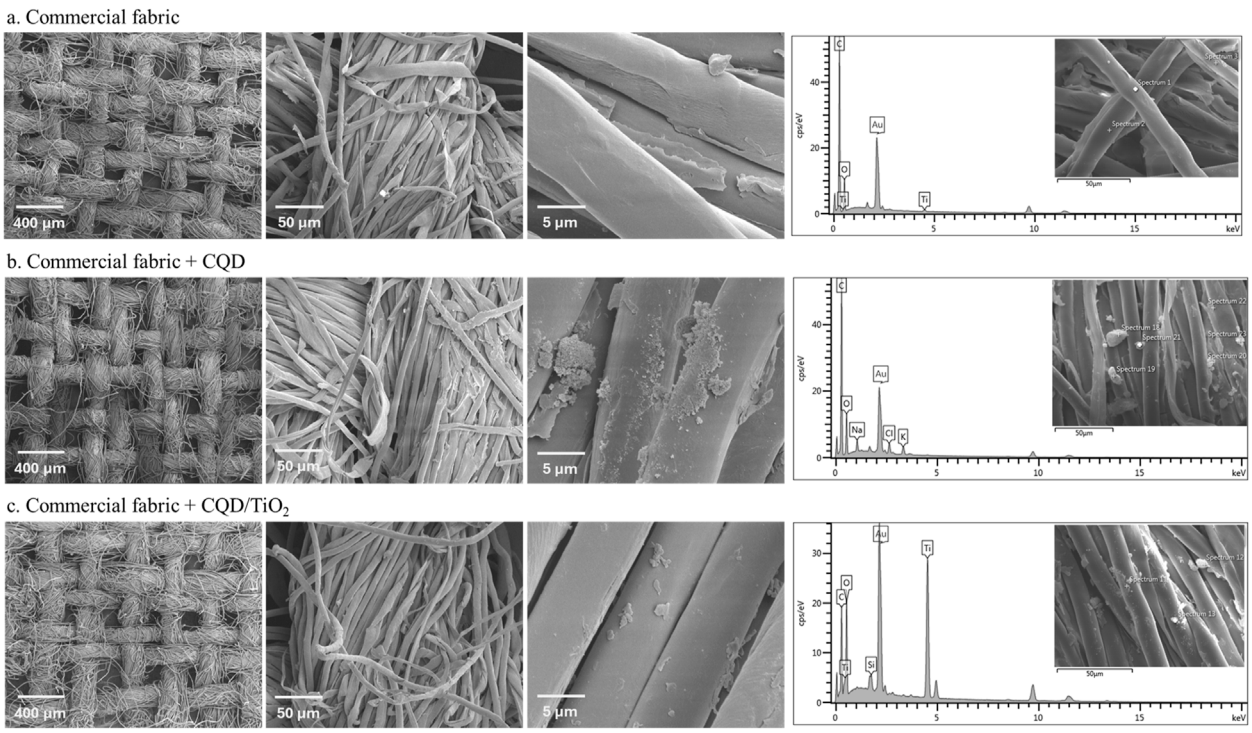

FIGURE 14
Scanning electron microscopy and EDS analyses of commercial cotton fabric impregnated with quantum dots: **(A)**. Neat commercial fabric; **(B)**. Commercial fabric with carbon quantum dots; and **(C)**. Commercial fabric with carbon quantum dots + TiO_2.

2013; Perotti et al., 2014; Lagarón et al., 2016; Venkateshaiah et al., 2020; Udayakumar et al., 2021), and it is repeated along the entire surface of the sample in a 3D arrangement. In Figure 15A, it is noticed that each microglobule has a smooth surface, and when the quantum dots are sprayed on the surface some agglomerations are evident on some globules, as well as an increase in the brightness of the perimeter of the same attributed to an overload of the sample due to the high content of organic material in the sample, which is favored by the preparation of this solution. As exposed previously, these aggregates correspond to a lack of dispersion of the carbon nanoparticles. Marked differences are observed in the results of the sample with 0.1% of quantum dots with TiO_2. A uniform distribution of the nanoparticles covers the entire surface of the microglobules along the entire sample surface, changing its smooth appearance to a rough surface as a result of the enhanced adherence of the nanoparticles to the sample.

As well as cotton fabric, the biopolymer mapping composition shows it is carbon-based, and the addition of TiO_2, which appears again at 4 keV in the EDS result, is much more noticeable than in commercial fabrics.

4 Conclusion

This work demonstrates the successful production of CQDs from nopal residues using a simple hydrothermal method. It was shown that the optical and physical properties of CQDs can be effectively tuned by adjusting the pH during synthesis. Notably, while pH significantly influenced the physical behavior of the CQDs, particularly in terms of colloidal stability and agglomeration, it also affected their absorption characteristics, resulting in distinct green-cyan and blue-cyan hues under UV light. However, the photoluminescence properties, including the peak excitation and emission wavelengths, remained relatively stable despite these variations. Emission wavelengths around 400 nm place the CQDs within the violet-blue spectrum, indicating their potential for applications requiring precise wavelength control, such as in optoelectronics, bioimaging, and sensing technologies.

The structural and optical characterization of CQDs synthesized under varying pH conditions revealed that pH significantly influences the functional groups and absorption properties of the CQDs. FTIR analysis indicated that higher pH levels enhance the presence of sp^2-hybridized C=C bonds, contributing to an extended absorption spectrum into the visible range. When integrated with TiO_2, the CQDs improved light absorption in the UV region, with spectroscopic studies demonstrating significant changes in the electronic structure. This interaction facilitated a phase transformation from anatase to rutile in TiO_2 as was evidenced by XRD results, suggesting that CQDs serve as effective nucleation sites that enhance material stability and material properties.

Furthermore, the successful impregnation of CQDs/TiO_2 onto textile materials, such as nopal and cotton fabrics, highlighted their potential for application in smart textiles. The photoluminescent properties observed under UV light indicate that these CQDs can act as effective fluorescent pigments, enhancing the functionality of textiles. Overall, this study emphasizes the importance of synthesis

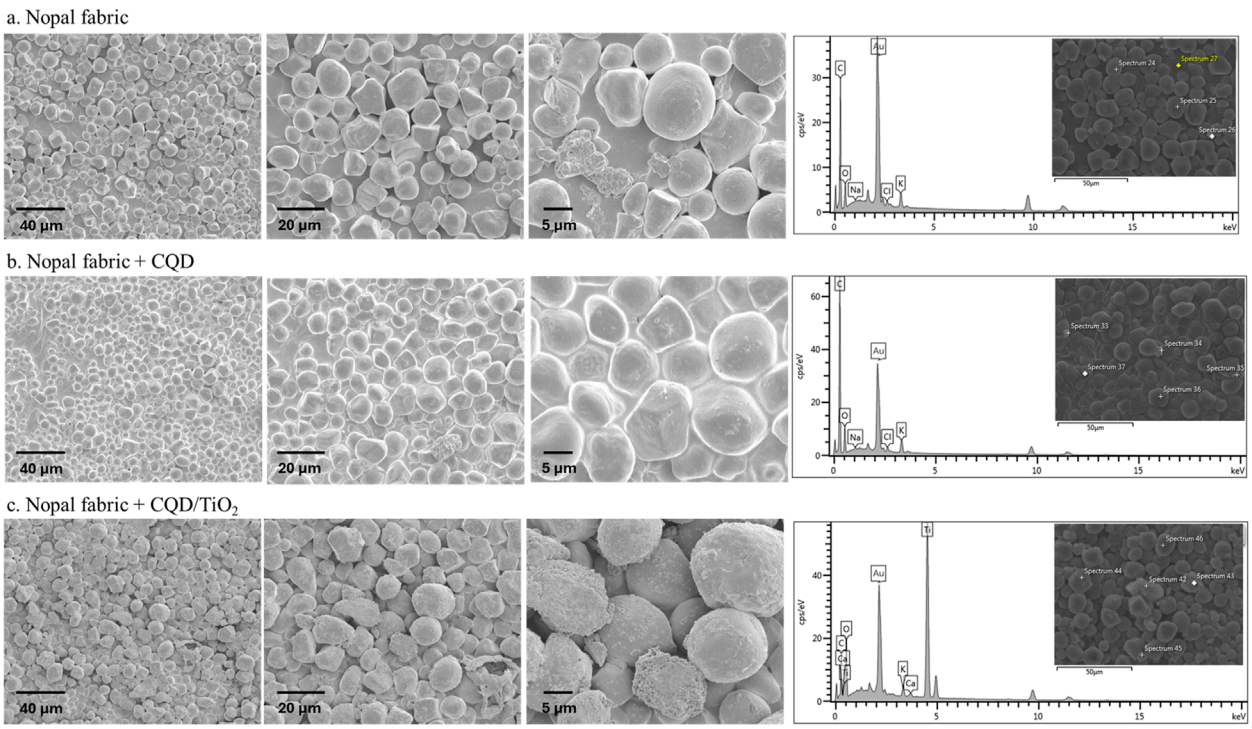

FIGURE 15
Scanning electron microscopy and EDS analyses of nopal fabric impregnated with quantum dots: **(A)**. Neat nopal fabric; **(B)**. Nopal fabric with carbon quantum dots; and **(C)**. Nopal fabric with carbon quantum dots + TiO_2.

conditions in tailoring CQD properties and their interactions with other materials, paving the way for innovative applications in textiles and beyond.

Moreover, the tunable optical properties, coupled with enhanced stability and quantum yield (58%), highlight the versatility of these CQDs for a range of applications, including bioimaging and environmental sensing. The ability to customize CQD characteristics through adjustments in synthesis conditions, such as pH and doping, further enhances their practical utility. Furthermore, the CQDs demonstrated pH-sensitive color changes, a feature that can be harnessed to create reversible colorimetric smart textiles. This, along with their fluorescence emissions and high light absorption efficiency, underscores the potential of these CQDs in revolutionizing smart textiles and optical sensing technologies.

Data availability statement

The raw data supporting the conclusions of this article will be made available by the authors, without undue reservation.

Author contributions

JM: Writing–original draft, Investigation, Formal Analysis, Data curation. EP-B: Writing–original draft, Methodology, Investigation, Data curation. VO-M: Writing–original draft, Data Curation, Formal Analysis, Investigation. MV-R: Writing–review and editing, Writing–original draft, Validation, Supervision, Methodology, Investigation, Formal Analysis, Data curation, Conceptualization. AF: Writing–review and editing, Writing–original draft, Validation, Supervision, Methodology, Investigation, Formal Analysis, Data curation, Conceptualization. NA: Writing–review and editing, Validation, Supervision, Project administration, Investigation, Funding acquisition, Formal Analysis, Conceptualization.

Funding

The author(s) declare that no financial support was received for the research, authorship, and/or publication of this article.

Acknowledgments

NA, MV, and AF thank Universidad de Medellín for the continuous support via internal projects. The authors also appreciate the facilities provided by the Grupo de Investigación en Fenómenos de Superficie Michael Polanyi at Universidad Nacional de Colombia. Special thanks to Instituto Tecnológico Metropolitano for their technical assistance with scanning electron microscopy. Also, the authors thank the Delfín program for the participation of students from different Mexican universities within the framework of the XXVIII Pacific Scientific and Technological Research Summer 2024.

Conflict of interest

The authors declare that the research was conducted in the absence of any commercial or financial relationships that could be construed as a potential conflict of interest.

Publisher's note

All claims expressed in this article are solely those of the authors and do not necessarily represent those of their affiliated organizations, or those of the publisher, the editors and the reviewers. Any product that may be evaluated in this article, or claim that may be made by its manufacturer, is not guaranteed or endorsed by the publisher.

Supplementary material

The Supplementary Material for this article can be found online at: https://www.frontiersin.org/articles/10.3389/fmats.2024.1478418/full#supplementary-material

References

Afroj, S., Karim, N., Wang, Z., Tan, S., He, P., Holwill, M., et al. (2019). Engineering graphene flakes for wearable textile sensors via highly scalable and ultrafast yarn dyeing technique. *ACS Nano* 13, 3847–3857. doi:10.1021/acsnano.9b00319

Agarwal, K., Rai, H., and Mondal, S. (2023). Quantum dots: an overview of synthesis, properties, and applications. *Mater Res. Express* 10, 062001. doi:10.1088/2053-1591/acda17

Akash, K., John P Paul Winston, A., Mohamed, K. M., Sagayaraj, P., Madhavan, J., Rajesh Kumar, S., et al. (2024). Efficacy of anti-inflammatory and antioxidant activities of carbon quantum dots synthesized from sugarcane bagasse and pith. *Inorg. Chem. Commun.* 169, 113046. doi:10.1016/j.inoche.2024.113046

Algadi, H., Albargi, H., Umar, A., and Shkir, M. (2021). Enhanced photoresponsivity of anatase titanium dioxide (TiO2)/nitrogen-doped graphene quantum dots (N-GQDs) heterojunction-based photodetector. *Adv. Compos Hybrid. Mater* 4, 1354–1366. doi:10.1007/s42114-021-00355-5

Algethami, K., Saidi, I., Ben Jannet, H., Khairy, M., Abdulkhair, B. Y., Al-Ghamdi, Y. O., et al. (2022). Chitosan-CdS quantum dots biohybrid for highly selective interaction with copper(II) ions. *ACS Omega* 7, 21014–21024. doi:10.1021/acsomega.2c01793

Arvapalli, D. M., Sheardy, A. T., Alapati, K. C., and Wei, J. (2020). High quantum yield fluorescent carbon nanodots for detection of Fe (III) ions and electrochemical study of quenching mechanism. *Talanta* 209, 120538. doi:10.1016/j.talanta.2019.120538

Ashraf, H., and Karahan, B. D. (2024). Biowaste valorization into valuable nanomaterials: synthesis of green carbon nanodots and anode material for lithium-ion batteries from watermelon seeds. *Mater Res. Bull.* 169, 112492. doi:10.1016/j.materresbull.2023.112492

Builes Vélez, A. E., Builes Escobar, N., Rossi, E., Mattram, A., Stocker, J., Rognoli, V., et al. (2022). Education for Sustainability approaching SDG 4 and target 4.7. *Editor. Univ. Pontif. Boliv.* doi:10.18566/978-628-500-077-5

Chang, C.-Y., Venkatesan, S., Herman, A., Wang, C.-L., Teng, H., and Lee, Y.-L. (2023). Carbon quantum dots with high quantum yield prepared by heterogeneous nucleation processes. *J. Alloys Compd.* 938, 168654. doi:10.1016/j.jallcom.2022.168654

Chauhan, D. S., Quraishi, M. A., and Verma, C. (2022). Carbon nanodots: recent advances in synthesis and applications. *Carbon Lett.* 32, 1603–1629. doi:10.1007/s42823-022-00359-1

Dhamodharan, D., Byun, H. S., Varsha Shree, M., Veeman, D., Natrayan, L., and Stalin, B. (2022). Carbon nanodots: synthesis, mechanisms for bio-electrical applications. *J. Industrial Eng. Chem.* 110, 68–83. doi:10.1016/j.jiec.2022.03.014

Ehtesabi, H., and Kalji, S. O. (2024). Carbon nanomaterials for sweat-based sensors: a review. *Microchim. Acta* 191, 77. doi:10.1007/s00604-023-06162-7

Ezati, P., and Rhim, J. W. (2022). Pectin/carbon quantum dots fluorescent film with ultraviolet blocking property through light conversion. *Colloids Surf. B Biointerfaces* 219, 112804. doi:10.1016/j.colsurfb.2022.112804

Felipe, B. H. S., Cabral, R. L. B., Ladchumananandasivam, R., Zille, A., Kim, S., Fechine, P. B. A., et al. (2022). Nanocoating on cotton fabric with nitrogen-doped graphene quantum dots/titanium dioxide/PVA: an erythemal UV protection and photoluminescent finishing. *J. Mater. Res. Technol.* 18, 2435–2450. doi:10.1016/j.jmrt.2022.03.078

Franco, C. A., Candela, C. H., Gallego, J., Marin, J., Patiño, L. E., Ospina, N., et al. (2020). Easy and rapid synthesis of carbon quantum dots from mortiño (vaccinium meridionale swartz) extract for use as green tracers in the oil and gas industry: lab-to-field trial development in Colombia. *Ind. Eng. Chem. Res.* 59, 11359–11369. doi:10.1021/acs.iecr.0c01194

Goswami, J., Barman, H., Hazarika, P., Manna, P., Devi, A., and Saikia, L. (2024). Biomass-derived phosphorous-doped carbon quantum dots (P-CQD): an excellent biocompatible material for *in-vitro* cell imaging. *Inorg. Chem. Commun.* 162, 112276. doi:10.1016/j.inoche.2024.112276

Hsieh, C.Te, Wu, F. L., and Yang, S. Y. (2008). Superhydrophobicity from composite nano/microstructures: carbon fabrics coated with silica nanoparticles. *Surf. Coat. Technol.* 202, 6103–6108. doi:10.1016/j.surfcoat.2008.07.006

Jia, L.-W., and Zhang, X. (2023). Versatile red-emissive carbon dots for smart textiles and fluorescence sensing. *ACS Appl. Nano Mater* 6, 1379–1385. doi:10.1021/acsanm.2c05012

Jin, Y., Tang, W., Wang, J., Ren, F., Chen, Z., Sun, Z., et al. (2023). Construction of biomass derived carbon quantum dots modified TiO2 photocatalysts with superior photocatalytic activity for methylene blue degradation. *J. Alloys Compd.* 932, 167627. doi:10.1016/j.jallcom.2022.167627

Lagarón, J. M., López-Rubio, A., and José Fabra, M. (2016). Bio-based packaging. *J. Appl. Polym. Sci.* 133. doi:10.1002/app.42971

Li, Z., Chen, R., and Zhang, L. (2013). Utilization of chitosan biopolymer to enhance fly ash-based geopolymer. *J. Mater. Sci.* 48, 7986–7993. doi:10.1007/s10853-013-7610-4

Ling, Y., Ji, Z., Tian, F., Peng, C., Wu, B., Liu, X., et al. (2022). Surface relaxation determine the band bending and special optical properties of carbon nanodots. *Surfaces Interfaces* 34, 102338. doi:10.1016/j.surfin.2022.102338

Lysenko, V., Kuznietsova, H., Dziubenko, N., Byelinska, I., Zaderko, A., Lysenko, T., et al. (2024). Application of carbon dots as antibacterial agents: a mini review. *Bionanoscience* 14, 1819–1831. doi:10.1007/s12668-024-01415-y

Lyu, J. S., and Han, J. (2024). Fabrication of bio-inspired carbon nanodot-corn starch nanocomposite films via extrusion process for sustainable active food packaging applications. *Carbohydr. Polym.* 343, 122502. doi:10.1016/j.carbpol.2024.122502

Mahmood, A., Shi, G., Wang, Z., Rao, Z., Xiao, W., Xie, X., et al. (2021). Carbon quantum dots-TiO2 nanocomposite as an efficient photocatalyst for the photodegradation of aromatic ring-containing mixed VOCs: an experimental and DFT studies of adsorption and electronic structure of the interface. *J. Hazard Mater* 401, 123402. doi:10.1016/j.jhazmat.2020.123402

Maiti, B., Wang, K., Bunge, S. D., Twieg, R. J., and Dunietz, B. D. (2020). Enhancing charge mobilities in self-assembled N···I halogen bonded organic semiconductors: a design approach based on experimental and computational perspectives. *Org. Electron* 79, 105637. doi:10.1016/j.orgel.2020.105637

Mansur, A. A. P., and Mansur, H. S. (2015). Quantum dot/glycol chitosan fluorescent nanoconjugates. *Nanoscale Res. Lett.* 10, 172. doi:10.1186/s11671-015-0879-2

Mirlou-Miavagh, F., Rezvani-Moghaddam, A., Roghani-Mamaqani, H., and Sundararaj, U. (2024). Comparative study of synthesis of carbon quantum dots via different routes: evaluating doping agents for enhanced photoluminescence emission. *Prog. Org. Coat.* 191, 108445. doi:10.1016/j.porgcoat.2024.108445

Ozyurt, D., Kobaisi, M.Al, Hocking, R. K., and Fox, B. (2023). Properties, synthesis, and applications of carbon dots: a review. *Carbon Trends* 12, 100276. doi:10.1016/j.cartre.2023.100276

Perotti, G. F., Tronto, J., Bizeto, M. A., Izumi, C. M. S., Temperini, M. L. A., Lugão, A. B., et al. (2014). Biopolymer-clay nanocomposites: cassava starch and synthetic clay cast films. *J. Braz Chem. Soc.* 25, 320–330. doi:10.5935/0103-5053.20130300

Pombo Barros, V. G. V. (2011). Puntos cuánticos: nueva aportación de la nanotecnología en investigación y medicina. *Rev. Complut. ciencias veterinarias* 5, 69–102. doi:10.5209/RCCV.23434

Quang, N. K., Hieu, N. N., Bao, V. V. Q., Phuoc, V. T., Ngoc, L. X. D., Doc, L. Q., et al. (2022). Hydrothermal synthesis of carbon nanodots from waste wine cork and their use in biocompatible fluorescence imaging. *Xinxing Tan. Cailiao/New Carbon Mater.* 37, 595–602. doi:10.1016/S1872-5805(22)60608-5

Rasal, A. S., Korupalli, C., Getachew, G., Chou, T. H., Lee, T. Y., Ghule, A. V., et al. (2021). Towards green, efficient and stable quantum-dot-sensitized solar cells through nature-inspired biopolymer modified electrolyte. *Electrochim Acta* 391, 138972. doi:10.1016/j.electacta.2021.138972

Rivera-Álvarez, A., Quesada-Ramírez, A., Vega-Baudrit, J., Paniagua, S. A., Rica, C., Rodrigo Facio, S., et al. (2021). Síntesis, propiedades y aplicaciones de puntos cuánticos a base de carbono.

Román, L. E., Huachani, J., Uribe, C., Solís, J., Gómez, M., Costa, S., et al. (2019). Blocking erythemally weighted UV radiation using cotton fabrics functionalized with ZnO nanoparticles *in situ*. *Appl. Surf. Sci.* 469, 204–212. doi:10.1016/j.apsusc.2018.11.047

Rosales, S., Zapata, K., Cortes, F. B., Rojano, B., Diaz, C., Cortes, C., et al. (2024). Simultaneous detection of carbon quantum dots as tracers for interwell connectivity evaluation in a pattern with two injection wells. *Nanomaterials* 14, 789. doi:10.3390/nano14090789

Sharma, S., and Chowdhury, P. (2024). Tunable dual photoluminescence from synthesized urea-based carbon quantum dots: a DFT based simulation on structural insights. *Opt. Mater (Amst)* 153, 115617. doi:10.1016/j.optmat.2024.115617

Sousa, H. B. A., Martins, C. S. M., and Prior, J. A. V. (2021). You don't learn that in school: an updated practical guide to carbon quantum dots. *Nanomaterials* 11, 611–688. doi:10.3390/nano11030611

Sun, J., Yan, K., Zhang, P., Pan, A., Xiong, W., Chen, X., et al. (2024). Fabrication of methylated carbon quantum dot-based fluorescent films for highly sensitive and stable temperature probes. *Colloids Surf. A Physicochem Eng. Asp.* 695, 134286. doi:10.1016/j.colsurfa.2024.134286

Tian, J., Leng, Y., Zhao, Z., Xia, Y., Sang, Y., Hao, P., et al. (2015). Carbon quantum dots/hydrogenated TiO2 nanobelt heterostructures and their broad spectrum photocatalytic properties under UV, visible, and near-infrared irradiation. *Nano Energy* 11, 419–427. doi:10.1016/j.nanoen.2014.10.025

Udayakumar, G. P., Muthusamy, S., Selvaganesh, B., Sivarajasekar, N., Rambabu, K., Banat, F., et al. (2021). Biopolymers and composites: properties, characterization and their applications in food, medical and pharmaceutical industries. *J. Environ. Chem. Eng.* 9, 105322. doi:10.1016/j.jece.2021.105322

Venkateshaiah, A., Padil, V. V. T., Nagalakshmaiah, M., Waclawek, S., Černík, M., and Varma, R. S. (2020). Microscopic techniques for the analysis of micro and nanostructures of biopolymers and their derivatives. *Polym. (Basel)* 12, 512. doi:10.3390/polym12030512

Wang, R., Zhang, S., Zhang, J., Wang, J., Bian, H., Jin, L., et al. (2024). State-of-the-art of lignin-derived carbon nanodots: preparation, properties, and applications. *Int. J. Biol. Macromol.* 273, 132897. doi:10.1016/j.ijbiomac.2024.132897

Yang, X., Lotfy, V. F., Basta, A. H., Liu, H., and Fu, S. (2024). Carbon quantum dots derived from rice straw doped with N and S and its nanocomposites with hydroxypropyl cellulose nanocomposite. *Int. J. Biol. Macromol.* 278, 134925. doi:10.1016/j.ijbiomac.2024.134925

Zamora-Valencia, C. A., Reyes-Valderrama, M. I., Salado-Lesa, D. E., and Rodriguez-Lugo, V. (2023). Síntesis hidrotermal de puntos cuánticos de carbono PEGilados. *Pädi Bol. Científico Ciencias Básicas Ing. del ICBI* 11, 35–43. doi:10.29057/icbi.v11iespecial5.11840

Zhao, H. (2019). Refractive index dependent optical property of carbon dots integrated luminescent solar concentrators. *J. Lumin* 211, 150–156. doi:10.1016/j.jlumin.2019.03.039

Zhao, L., Zhang, P., Li, L., Li, N., Tuerhong, R., Su, X., et al. (2024). Revealing the potential of quantum dot nanomaterials in photocatalytic applications. *Chemosphere* 361, 142547. doi:10.1016/j.chemosphere.2024.142547

Zhu, S., Meng, Q., Wang, L., Zhang, J., Song, Y., Jin, H., et al. (2013). Highly photoluminescent carbon dots for multicolor patterning, sensors, and bioimaging. *Angew. Chem. - Int. Ed.* 52, 3953–3957. doi:10.1002/anie.201300519